International Journal of Engineering Trends and Technology
ISSN: 2231-5381/ https://doi.org/10.14445/22315381/IJETT-V74I3P114

Volume 74 Issue 3, 181-199, March 2026

Original Article

Optimization of Ocular Cancer Anomaly Detection using Generative AI-based Multi-Scale Transformation Model

Sumalatha Aradhya[1], Nehal Revuri[2]

[1,2]*Department of Computer Science and Engineering, Siddaganga Institute of Technology, Tumakuru, Karnataka, India.*
[2]*Dublin High School, California, United States.*

[1]*Corresponding Author : sumalatha@sit.ac.in*

Received: 27 October 2024 Revised: 02 February 2026 Accepted: 06 February 2026 Published: 28 March 2026

Abstract *- Ocular Disease affects millions of people, and if not treated in advance, it may cause vision loss. The traditional way of detecting the disease is not accurate due to image filtering issues. In this paper, an optimal algorithm to improve diagnostic accuracy is proposed. The proposed framework facilitates ease of use, an intuitive interface to scan the eye images, to analyze the images, and to generate a comprehensive report of disease classifications and predictions using a generative AI-based multi-scale transformer model. The results obtained prove that the proposed system achieves the highest level of Accuracy in detecting and diagnosing eye diseases. The proposed solution uses the Visual Transformation Technique (VIT), and the proposed model eases the detection and diagnosis of eye diseases and cancer cells with an accuracy of 99.9%. The developed solution can be used by the ophthalmologist to ensure that patients receive prompt and accurate treatment, irrespective of the localities where there are fewer facilities, to accurately detect multiple anomalies.*

Keywords *- Gen AI, Transformer Models, ViT, VGG19, Ocular Cancer Cell, Anomalies Detection, Optical Coherence Tomography (OCT).*

1. Introduction

The detection of cancer cells or ocular diseases can be found using tomography [1]. Tomography is used in the standard detection of cancer cells and ocular diseases. Furthermore, to diagnose vision-threatening retinal disorders, precise choroid measurements are required. However, precise automation of choroid segmentation remains a significant challenge. This paper introduces an optimized filtering approach based on a Deep Learning algorithm to segment images quickly and accurately in the absence of human involvement. Deep learning techniques and algorithms were used to detect disease from various medical scans. Namely, ResNet50 and VGG19 were utilized to analyze and predict such anomalies. The extracted image set and patches are filtered by increasing the contrast and intensity of the region of interest. VGG19 is a simple yet effective design, utilizing 3x3 filters and stacking layers, making it a conventional option to classify images and transfer learning tasks [2]. There will be skipping connections in VGG19, as found in ResNet50, hence the Accuracy will be higher, causing a preference for VGG19 over ResNet50. However, this method risks lower efficiency.

1.1. Cancer of the Eye

Studies estimate that tens of millions of people worldwide develop either eye disease or eye cancer annually. In many cases, there is a significant probability of vision impairment. In fact, the primary cause of vision loss is due to undiagnosed cancer cells across the retinal area [3, 4]. Tomography is used to detect ocular diseases. However, eye disease and eye cancer often become difficult to detect in day-to-day life, as symptoms may be associated with reactions to pollution and dust [5]. A total of five different diseases or stages of the eye are considered, particularly Retinoblastoma, Myopia, Cataract, Hypertension, and Glaucoma [6].

1.2. Causes of Eye Cancer

The causes of eye cancers are varied and often involve a complex interplay of genetic, environmental, and lifestyle factors. Genetic predisposition plays a significant role, particularly in conditions like Retinoblastoma. This Cancer can be inherited through mutations in the RB1 gene, which are present from birth and significantly increase the risk of developing the disease. Families with a history of Retinoblastoma or other genetic disorders might find themselves at higher risk, making genetic counselling and regular screenings essential for early detection and management [7]. UV radiation is another well-documented risk factor, especially for cancers affecting the outer parts of the eye, such as conjunctival squamous cell carcinoma. The risk highlights the importance of wearing protective

sunglasses and hats to shield the eyes from excessive UV exposure, particularly for those spending significant time outdoors or living in areas with high UV index [8]. Exposure to Ultraviolet (UV) radiation, often from sunlight or tanning beds, is a well-established risk factor for various types of eye cancers. Additionally, some studies have suggested that exposure to certain chemicals in the occupations of welding and painting may potentially increase the risk of a type of eye cancer known as uveal melanoma [9].

Viral infections have also been implicated in some cases of eye cancer. Human Papillomavirus (HPV), for example, is associated with Conjunctival Papilloma and, in rarer cases, squamous cell carcinoma of the conjunctiva. HPV can be contracted, and its association with eye cancer highlights the need for vaccination and preventive health measures [10]. Additionally, the Epstein-Barr virus (EBV) has been linked to primary Intraocular Lymphoma, emphasizing the role of viral infections in eye cancer development. Although both have been established in studies to increase risk for eye cancers, apparently, EBV has had more evidence [11]. Age and gender can influence the risk of developing eye cancer. For instance, Retinoblastoma predominantly affects young children, while uveal melanoma is more common in adults, particularly those over 50 [12].

Finally, systemic conditions and other cancers can influence the risk of eye cancer. For example, individuals with a history of skin cancer, such as basal cell carcinoma, may have an increased risk of developing ocular malignancies due to shared risk factors like UV exposure [13]. Moreover, certain systemic diseases, such as Neurofibromatosis Type 1, can predispose individuals to eye tumours [14]. Gender differences also exist, with some studies suggesting that men may have a slightly higher risk for certain types of eye cancer. However, the reasons for this disparity are still under investigation. Awareness of these demographic factors can aid in targeted screening and preventive strategies. Symptoms of eye cancers can vary widely, from vision changes and eye pain to visible lumps or discoloration. Because of this variability, regular eye exams are crucial [15, 16]. If any abnormalities are detected, further testing like ultrasounds, MRIs, or biopsies might be necessary to confirm the diagnosis [17].

1.3. Treatments

Treatment approaches for eye cancers can vary depending on the type and stage of the disease. Uveal melanoma is commonly addressed with Brachytherapy (internal radiation therapy), external beam radiation, or surgery to remove part of the eye [31, 32]. Additionally, laser therapies such as Transpupillary Thermotherapy (TTT) can be employed [33]. Conjunctival melanoma is typically managed through surgery, cryotherapy (freezing therapy), and topical chemotherapy eye drops [34]. Lymphoma of the eye is treated using radiation therapy or chemotherapy, depending on the specific case [35]. In the case of Retinoblastoma, options include cryotherapy, laser therapy, chemotherapy, surgery, and radiation therapy [36]. For eyelid cancers like basal and squamous cell carcinomas, treatments may involve surgery (including Mohs surgery in some cases), cryotherapy, topical chemotherapy creams, radiation therapy, or photodynamic therapy [37]. Orbital and adnexal cancers are treated with a combination of surgery, radiation therapy, and sometimes chemotherapy [38].

For advanced or metastatic eye cancers, more targeted treatments are utilized, such as immunotherapy (e.g., tebentafusp for uveal melanoma), targeted therapies aimed at specific genetic mutations, and liver-directed therapies for metastases [39, 40]. The range and diversity of these treatments demonstrate the complexity and precision required in managing eye cancers, emphasizing the complexity of different approaches.

The key to effective treatment is early diagnosis, which is critical for eye cancers. For early detection, screening programs often include detailed eye examinations by an ophthalmologist, helping to detect subtle structural eye changes [41]. Concentrated spots of tissue of a different color may also mark cancerous growth, which can be observed in a biopsy [42]. For high-risk populations, including children with a family history of Retinoblastoma, specialized screenings and genetic counselling are recommended [43]. Advances in imaging technology, such as Optical Coherence Tomography (OCT) and fundus photography, have also enhanced the ability to detect eye cancers at their earliest stages, allowing for timely intervention and a better prognosis [44].

OCT utilizes light waves to depict detailed images of the retina and choroid [45]. Ultrasound (namely B-scan ultrasonography) is commonly used to visualize tumors within the eye, providing their location, size, and shape [46]. Fluorescein Angiography involves injecting dye to highlight blood vessels in the eye, which helps to isolate and differentiate melanoma [32].

Magnetic Resonance Imaging (MRI), Computer Tomography (CT), and Positron Emission Tomography (PET) are also being utilized to detect metastasis of eye cancers beyond the region of the eye, assisting in the tracking and management of eye cancers over time. Table 1 illustrates classification types and the existing approach to identifying eye cancer.

The paper is organized as follows. Section 2 illustrates the approaches and limitations of existing or related works. Section 3 covers the proposed methodology, and Section 4 depicts the results obtained. Future scope and conclusions are highlighted in Section 5.

Table 1. Classification of eye cancers

Ocular Cancer Type	Ocular Region	Findings	Reference/s
Uveal Melanoma: Prevalent Intraocular Cancer in Adults	Uvea	Review Article on Eye Cancer: Ocular oncology research is conducted extensively, and stepwise regulation is suggested.	Harbour, J. W. et.al (2006) [18], Ali Hazazi et.al (2024) [19]
Iris Melanoma: A Subtype of Uveal Melanoma, often grows slowly	Iris	Review article on Recent developments in management of ocular melanoma. The work emphasizes the cytogenetic study of Metastatic disease and suggests prioritization of Treatments	Bilmin et. al. (2021) [20] Barbi, Mali MD (2024) [21]
Ciliary Body Melanoma: Subtype of uveal melanoma	Ciliary body	Review article on Ocular oncology: Advances in Retinoblastoma, uveal melanoma, and conjunctival melanoma. A study on choroidal melanoma, genetic analysis is explained, and management of patients is suggested.	Damato, B., & Singh, A. D. (2019) [22], Marina et. al [23]
Choroidal Melanoma: Most common subtype of uveal melanoma	Choroid	The paper proposes the application of advanced nanoparticles for imaging and therapy.	Bilmin et. al. (2021) [20]
Retinoblastoma: The most common primary intraocular Cancer in children	Retina	Lecture/Review article on Eye Cancer. The critical pathway governing Retinoblastoma is illustrated, with clinical and therapeutic implications.	[18, 19]
Conjunctival Melanoma: Rare, aggressive form of eye melanoma	Conjunctiva	Review article. Advances in the Management of Retinoblastoma, uveal melanoma, and conjunctival melanoma are discussed in the paper.	[22, 23]
Conjunctival Squamous Cell Carcinoma: Most Common Conjunctival Cancer	Conjunctiva	Review article. Radiotherapy and the application of topical agents are proposed in the paper.	Höllhumer, R. et al (2021) [24], Sitong Ju et. al. (2024) [25]
Primary Intraocular Lymphoma: Rare, often associated with CNS lymphoma	Inside the eye	Clinical practices are explained in the paper on Ophthalmic Oncology with advances in The Management of Ocular Tumors. The proposed approach focuses on targeted therapy and prioritizing the alignment of oncological principles with life	Anguita, R et al [26], Mrittika Sen et. al. (2024) [27], Sara Verbeek et. al. (2024) [28]
Orbital Rhabdomyosarcoma, Lacrimal Gland: Soft tissue sarcoma, mainly affects children, Eyelid Sebaceous Carcinoma	Tissues around the eye, Eyelid	Remarks on clinical practices in Ophthalmic Oncology are illustrated in the paper. The targeted therapy is proposed for the management of carcinoma.	[26-28]
Eyelid Basal / Squamous Cell Carcinoma: Among most Common eyelid malignancies	Eyelid	Update/Review article on Ocular Oncology. Surgical and medical management, and an overview of topical therapy, are suggested in the paper.	[24, 25]
Optic Nerve Glioma: Observed in Children with Neurofibromatosis	Optic nerve	Neoadjuvant systemic immunotherapies are proposed to treat cancers	
Eyelid Melanoma: A Rare form of eyelid cancer	Eyelid	A review article summarizing recent developments in the management of ocular melanoma is discussed.	Garbe C et al (2022) [29] Kulbay et al. (2024) [30]

Furthermore, other techniques needed to find limitations of the eye and eye angiography can provide additional details about tumor location and blood vessel involvement [47]. Eyelid tumors, a particularly challenging cancer to detect and treat early, can be more frequently detected with regular skin cancer screenings [48]. Most of these techniques are used in

combination with others to effectively improve patient outcomes, and specific tests, like skin cancer readings and Fluorescein Angiography, might be used to detect certain classifications of eye cancer more than others. Combinations of tests may be employed depending on individual cases and clinical intuition.

1.4. ML in Imaging Analysis

After screening, image segmentation is one of many techniques used to analyze images produced by certain imaging scans. AI-based image segmentation can automatically delineate specific anatomical structures in complex eye images, isolating potential tumor sites and enabling more accurate analysis. This method enhances the precision of high-speed diagnoses and increases the scope and applicability of targeted therapies. An image segmentation can be clustered, extracted, and analyzed effectively by applying unsupervised machine learning models and by using UNet-based approaches as suggested by Lai, W et.al. [49].

Images are frequently analyzed by AI and ML techniques, which have demonstrated commendable performance with Accuracy exceeding that of physicians [50]. One of the most prominent techniques used in eye cancer detection is Convolutional Neural Networks (CNNs), Deep Learning models that excel at image analysis. Their capability in image analysis makes them well-suited for the evaluation of complex images of the eye, including fundus photographs, OCT scans, and histopathological images [51]. CNNs can be trained to recognize any outlying lesions, classify types of tumors, and predict the malignancy of a select tumor based on visual patterns. This process accounts for details that may be overlooked by physicians [52].

Transfer learning is another important technique in the realm of specific task-based model training. This approach to training allows for effective results despite the scarcity of large, annotated datasets. It adapts existing models trained on broader datasets, and as a result, produces high levels of Accuracy even with limited data [53]. Specifically having to do with image analysis, there are various methods: feature extraction, texture analysis, and morphological operations, all helping to enhance relevant features in eye images and suppress any noise or distractions.

AI presents a powerful tool in image classification. The first step to the development and integration of any AI model is the collection of massive amounts of data for preprocessing and training. Then, the model is selected, and it undergoes architecture design. Training and validation soon follow, and performance evaluation utilities metrics like Accuracy, sensitivity, and specificity. The model's conclusions are then interpreted and described by professionals, which assists in improving the explainability of the model's future versions. Finally, the mode undergoes clinical integration and continuous monitoring. Advanced machine learning techniques complement traditional screening methods, demonstrating potential for a greater improvement in the Accuracy and efficiency of eye cancer detection.

1.5. Segmentation and Detection Techniques

The fovea is a minor depression within the neurosensory retina, and visual acuity is at its highest level. The UNet method is used to localize a pixel-wise regression task using the fovea centralis. Nearly 5586 OCT volumes from 154 eyes are considered to analyze the fovea [54, 55]. Neovascularization is a process that happens in the human body when a new blood vessel grows.

The prime location for the occurrence of Neovascularization is in the eye, which includes the cornea and retina. The side effects of these newly grown vessels include leak, blurry vision, and, most fatally, vision loss. Miura, G. et.al have found a solution to detect Neovascularization [56]. Retinopathy screening is a non-invasive approach for collecting retinal pictures and is used for detecting Neovascularization from retinal images [57].

To identify Neovascularization, the network uses the Feature Pyramid Network and Vovnet as its backbone. Color fundus pictures from practice were used to assess the network. According to the experimental results, the network requires less training and testing time than Mask R-CNN while maintaining a high accuracy of 98.6% [58].

OCT is used to see the structure of the eyes. One needs to keep one's eyes still during this imaging technique. OCT uses IR light and measures the amount of optical capacity [59]. The ocular location is unclear in the two-dimensional mode [60]. The ASTRA toolbox is a framework for constructing OCT images. Reconstruction, forward and backward propagation across the projection domain, is mapped using the toolbox [61].

The super pixels were extracted using the Preoperative OCT to predict the acuity in human vision [62]. The extracted patches are then improved by raising the contrast of the infected area, and then loaded into a CNN for classification. The collected results proved the suggested segmentation method's efficacy in terms of accuracy [63]. The concept of Back Propagation was used while training the data to minimize the errors and thereby generating more accurate results [64]. The localization of a pixel is a regression task, and the Neural Network uses the Tensor Ring Decomposition method [65] and FIT-Net [66] as its backbone. However, the Accuracy of feature extraction and Anomaly Detection (AD) is lower. Hence, an effective and more accurate deep learning framework-based multiscale Anomaly detection for automated identification of ocular cancer cells is proposed in the paper.

The importance of evaluating the segmentation techniques in radiographic images is detailed in the paper authored by M. Thirugnanam et. al. [67]. The study focused on the Region of Interest containing defects, and it is suggested to develop a unified segmentation technique. Classification techniques of fundus images are proposed in the paper authored by O. Bernabé et.al [68], and the application of semi-supervised learning is detailed in the paper authored by S. Li et. al [69]. The fusion of labeled and unlabeled data approach is helpful in carrying out the classification of images. Clinical data were considered for the tomographic analysis and AI-based grading system proposed by M. Elsharkawy et.al [70] and Panayides S A et.al [71]. However, the analysis was to determine age-related information. The need for detection at the earlier stages of infection is detailed in the survey study mentioned in the paper authored by Guangming et. al. According to the authors, the usage of Artificial Intelligence will address the challenges and can predict the defects in advance [72]. High-quality speckle-free 3D-based unsupervised Deep Learning is proposed by Chen et. al. [73], and the results are impressive. The experiment was carried out on OCT images of meat, but not on ocular.

A constraint-based optimization to reconstruct multiple images by fetching a basis region is proposed for medical OCT applications by Ling Y et.al [73, 74]. The result shows that the reconstruction is accurate, and such a region clipping method is inherited in our research work. MTANet-based Deep Learning framework is proven to be the best among the other Neural Networks [74] for lung cancer detection. However, their approach to detecting multiple anomalies remains a challenge.

For the heterogeneous big data set, integration approaches are proposed by Amit et.al [75], and the survey suggests the best approaches for managing the massive data set. The volume, velocity, variety, veracity, and value parameters are considered for the practical analysis of the data. Analytics on data-intensive technology and usage of machine learning algorithms on health care data are discussed in the paper authored by K. Venkatram et.al [76]. It is suggested to preprocess and normalize the data for better Accuracy. A Deep Learning model for image classification, image reconstruction, and image formation is proposed by Yuwen X et al. Al [77] and Grewal S Mohinder et.al [78]. However, the existing approaches lack Accuracy.

1.6. Anomaly Detection and the ViT Model

The Anomaly Detection (AD) approach itself is fundamentally different from traditional classification methods. Rather than training the model to recognize specific disease patterns, it is trained exclusively on normal images to learn the intricate details of healthy eyes. During the inference phase, the model identifies deviations from these learned standard patterns as potential anomalies. This approach is particularly valuable for detecting rare conditions or novel presentations of diseases that may not be well-represented in traditional supervised learning datasets [79].

The unsupervised nature of AD tackles the challenge of low-frequency eye cancer data availability, detecting a wide range of anomalies without requiring extensive datasets detailing each pathology [80]. To enhance the model's performance and reduce training time, transfer learning techniques are employed. CNN is initially trained on a large, general image dataset, which allows it to develop a broad understanding of visual features. This pre-trained network is then fine-tuned on the specific eye image dataset, enabling it to adapt its learned features to the nuances of retinal images. This approach significantly reduces the amount of task-specific training and data required, and often leads to improved generalization capabilities [81].

Eye cancer AD, a cutting-edge application of artificial intelligence in ophthalmology, offers an auspicious approach to early diagnosis and improved patient outcomes. This category of screening leverages advanced machine learning to analyze retinal images and identify potential ocular malignancies (especially uveal melanomas), which are often challenging to detect in early stages. The following sections delve into the core methodology of eye cancer AD, especially in the context of Vision Transformers (ViT). Image classification occurs in layers, where, conventionally, researchers and scientists have used Convolutional Neural Networks (CNNs). Modeled based on the visual perception in animals, CNNs are integral tools predominantly utilized in image classification, distinguishing them as a crucial application of modern Deep Learning. Due to the abundance of extensive training data and access to computational resources, it becomes possible to train highly advanced CNNs in complex image and video classification, tenets of AI's application in healthcare today [82, 83].

1.7. Performance Criteria

Rigorous performance evaluation is conducted to assess the model's effectiveness in detecting eye cancer anomalies. Key metrics such as the area under the receiver operating characteristic curve, Accuracy, and F1 score are utilized to quantify the model's ability to distinguish between normal and anomalous eye images. These metrics provide a comprehensive view of the model's performance, balancing its ability to correctly Identify Anomalies (sensitivity) with its ability to avoid False Positives (specificity). Continuous evaluation and refinement of the model based on these metrics ensures its reliability and applicability in clinical settings.

1.8. Comparing ViT with Other Models

ViTs are models that were initially utilized in Natural Language Processing (NLP); however, recent studies have demonstrated their potential in image classification. With

results even surpassing those of CNNs, ViT models differ significantly from competitors in their architecture. As opposed to using convolutional layers to extract features from images, ViT models treat images as sequences of patches and use self-attention mechanisms from transformer architectures.

A lightweight CNN captures global relationships and forms connections [84, 85]. ViTs involve dividing an input image into fixed-size patches, which are then flattened and linearly embedded. Position embeddings are added to retain spatial information, where the resulting sequence is produced through layers of self-attention and feed-forward neural networks. Such methodology enables the ViT to focus on relevant features regardless of their spatial location, a valuable asset especially in the context of identifying subtle and distributed signs of disease. The recent implementation of ViT for cancer detection has produced promising results.

In ophthalmology, ViT-based models have demonstrated proficiency in detecting multiple retinal diseases, including Retinoblastoma, particularly from fundus photographs. Models such as these display the capability to focus on relevant image areas without explicit guidance, a valuable feature since precise lesion localization can prove to be and often is challenging.

Although the current data is limited to the efficacy of ViT models in eye cancer detection, there are studies that support its applicability in breast cancer detection from mammograms, skin lesion classification (i.e., melanoma), and lung nodule detection from mammograms. The ViT evaluations are primarily based on different cancers since their application in eye cancer AD is still limited [85]. In a study conducted by Nishigaki et al, the effectiveness of ViT classification of PET/CT images as benign or malignant was apparent, with an AUC curve of 90%, outperforming CNN models like EfficientNet and DenseNet (both of which exhibit an AUC value of 87%) [86]. In many cases, ViT-based approaches are outperforming traditional CNN models, mainly in the detection of subtle changes in eye conformation. ViTs have also proven usage in osteoporosis detection from X-ray images, as evaluated by a study that conducted a comparative analysis of ViTs and CNNs in osteoporosis detection. The study showed how ViT models generally outperformed CNN models. The best-performing ViT model (vit_s16) surpassed the top CNN model (VGG19) with a statistically significant difference of $p = 0.036$ [86]. ViTs demonstrate ample efficacy in medical image analysis tasks involving anomaly detection.

2. Materials and Methods

2.1. Proposed Framework

The proposed framework takes OCT images, or user-provided ocular images, and recursively applies image preprocessing to the input feed. The image transformation, scaling, mapping, clipping, and reconstruction are performed on the image dataset. Fetching the region of interest to identify anomalies is performed at the Feature Extraction layer.

Image transformation is carried out to the next level, and then image reconstruction is performed using a novel filtering algorithm. The proposed framework uses the ViT Transformation Deep Learning network model to train and test the processed images. Image classification is done as a set of anomalies as per the infected area segregation. An infected ocular cell may have one or more anomalies.

The proposed framework categorizes the anomalies identified as one anomaly if one patch of infected area is found, two anomalies if an infected cell has two patches, and multiple anomalies if a greater number of patches are found. In case of no anomalies, the ocular cell is classified as normal. The proposed framework to detect the images shown in Figure 1.

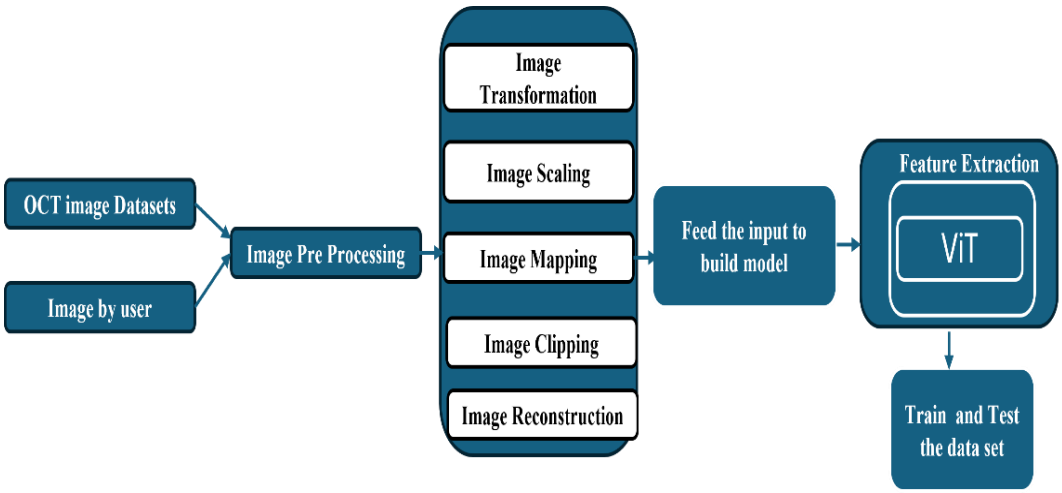

Fig. 1 Proposed framework

2.2. Mathematical Model to Fetch the Region of Interest

With the stepwise iterations of Image Transformation, Image Scaling, Image Mapping, Image Clipping, and Image Reconstruction, the region of interest is fetched. A mathematical model is applied at the preprocessing stage. The derivation of the reconstruction of the image before feature extraction is performed as per (1) to (17). To maintain the coordinate value of each vertex i, scaling is used to produce transformed coordinates (xi', yi').

$$x_i' = x_i.Scale_{xi} \ , y_i' = y_i.Scale_{yi} \tag{1}$$

where: Scalexi is a scaling factor to scale objects in the x direction, Scaleyi is a scaling factor to scale objects in the y direction. relative object proportions with unequal values, a differential scaling is used. Suppose (xi, yi) is a direction. In matrix form, the transformation is written as in (2).

$$\begin{bmatrix} x_i' \\ y_i' \end{bmatrix} = \begin{bmatrix} Scale_{xi} & 0 \\ 0 & Scale_{yi} \end{bmatrix} \cdot \begin{bmatrix} x_i \\ y_i \end{bmatrix} \tag{2}$$

The representation of scaling shown in Figure 2.

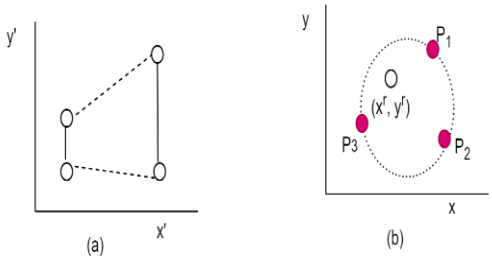

Fig. 2 Image scaling representation for transformation point

Polygon transformation points with respect to relative scaling are calculated as in (3).

$$\begin{aligned} x_i' &= x_i^r + (x_i - x_i^r) \cdot Scale_{xi} \ , y_i' \\ &= y_i^r + (y_i - y_i^r) \cdot Scale_{yi} \end{aligned} \tag{3}$$

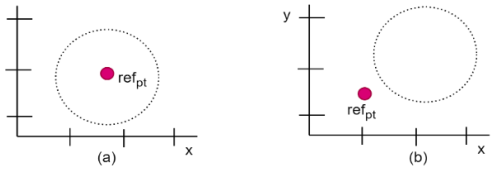

Fig. 3(a) Is transformed with reference point into, and (b) by composite

An anomaly detected area is first tested with the overlapping neighbor window before the next iterative steps, as shown in Figure 4.

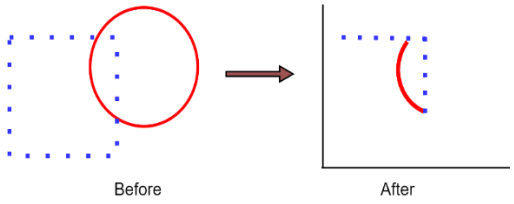

Fig. 4 Anomaly defection region clipping

The matrix with reference points represented as in (4).

$$V_i' = A_1 \cdot V + A_2 \tag{4}$$

Where: V_i, V_i': Column vectors, A1: 2 × 2 array with multiplicative factors, A2: 2-element columns with translation terms. The rotation transformation equation is calculated as per (5).

$$\begin{bmatrix} x_i' \\ y_i' \\ 1 \end{bmatrix} = \begin{bmatrix} cos\theta & -sin\theta & 0 \\ sin\theta & cos\theta & 0 \\ 0 & 0 & 1 \end{bmatrix} \cdot \begin{bmatrix} x_i \\ y_i \\ 1 \end{bmatrix} \tag{5}$$

Then, the scaling transformation is relative to the coordinate origin given by (6)

$$\begin{bmatrix} x_i' \\ y_i' \\ 1 \end{bmatrix} = \begin{bmatrix} Scale_{x_i} & 0 & 0 \\ 0 & Scale_{y_i} & 0 \\ 0 & 0 & 1 \end{bmatrix} \cdot \begin{bmatrix} x_i \\ y_i \\ 1 \end{bmatrix} \tag{6}$$

Successive rotations are applied to get the transformed function. With two successive scaling operations on the coordinates, the matrix is updated as in (7).

$$\begin{bmatrix} Scale_{x_i} & 0 & 0 \\ 0 & Scale_{x_i} & 0 \\ 0 & 0 & 1 \end{bmatrix} \cdot \begin{bmatrix} Scale_{x_i} - 1 & 0 & 0 \\ 0 & Scale_{y_i} - 1 & 0 \\ 0 & 0 & 1 \end{bmatrix} \tag{7}$$

Applying iterative operations of transformations, rotations, and scaling, a two-dimensional transformation matrix is represented as in (8)

$$\begin{bmatrix} x_i' \\ y_i' \\ 1 \end{bmatrix} = \begin{bmatrix} rScale_{x_i} & rScale_{x_i} & rScale_{x_i} \\ rScale_{x_i} & rScale_{x_i} & rScale_{x_i} \\ 0 & 0 & 1 \end{bmatrix} \cdot \begin{bmatrix} x_i \\ y_i \\ 1 \end{bmatrix} \tag{8}$$

The transformed coordinators are calculated as in (9)

$$x_i.rScale_{y_ix_i} + y_i.rScale_{y_iy_i} + t.rScale_{y_i} \tag{9}$$

The transformed matrix gets the value as in (10)

$$A_{1,1} = Scale_{x_i} ,$$

$$A_{1,3} = \left(1 - Scale_{x_i}\right) \times ref_{pt} \times x_i$$

$$A_{2,2} = Scale_{y_i},$$

$$A_{2,3} = (1 - y_i) \times ref_{pt} \times y_i \quad (10)$$

Where: $xref_{pt}$ is given by (11)

$$x_{ref_{pt}} = A_{1,1} \times x_I + A_{1,2} \times y_I + A_{1,3}, y_{ref_{pt}}$$

$$= A_{2,1} \times x_I + A_{2,2} \times y_I + A_{2,3} \quad (11)$$

$A_{1,1}$ and $A_{2,1}$ are transformed vectors with values, $A_{1,2}$ = -sin(θ) and $A_{2,1}$ = sin(θ), and the shapes are transformed with reference point as shown in Figure 3. To scale up to actual window mapping area, the new scaling factors are derived as shown in (12).

$$w_{S_x} = \frac{(wx_{imax} - wx_{imin})}{(wx_{jmax} - wx_{jmin})}, w_{S_y}$$

$$= \frac{(wy_{imax} - wy_{imin})}{(wy_{jmax} - wy_{jmin})} \quad (12)$$

Accordingly, defect detection regions using curve clipping operations are obtained if the following inequalities as per (13) are met.

$$x_{imin} \leq x \leq x_{imax}, y_{imin} \leq y \leq y_{imax} \quad (13)$$

where: (x_{imin},x_{imax}, y_{imin},y_{imax}) are the edges of the detected region. The coordinate extents of individual segments of anomaly areas are considered first. Then, the curve region intersections are calculated. Multiple passes are applied in regions. On the first pass, the mapped area is clipped. If there is an intersection, then simultaneous curve equations are applied to obtain the mapping intersection regions. To produce a display of 3D objects, input data sets are processed through multiple iterations of rendering processing inclusive of operations such as scaling, clipping, mapping and transformations. The linear plane equations with successive coordinates are applied as per (14).

$$\left(\frac{U}{\Delta}\right) x_i + \left(\frac{V}{\Delta}\right) y_i + \left(\frac{W}{\Delta}\right) z_i = -1 \quad (14)$$

where:

k = 1, 2, 3

(U, V, W) represents constants and coefficients of spatial properties of surface (x, y, z) represents any point in surface. Δ represents displacement constant coefficient of planes. Then, using Cramer's rule [39], obtain (15) and (16).

$$U = \begin{vmatrix} 1 & y_1 & z_1 \\ 1 & y_2 & z_2 \\ 1 & y_3 & z_3 \end{vmatrix} V = \begin{vmatrix} x_1 & 1 & z_1 \\ x_2 & 1 & z_2 \\ x_3 & 1 & z_3 \end{vmatrix}$$

$$W = \begin{vmatrix} x_1 & y_1 & 1 \\ x_2 & y_2 & 1 \\ x_3 & y_3 & 1 \end{vmatrix} \Delta = \begin{vmatrix} x_1 & y_1 & z_1 \\ x_2 & y_2 & z_2 \\ x_3 & y_3 & z_3 \end{vmatrix} \quad (15)$$

The value of each coefficient is calculated as [40],

$$U = y_1(z_2 - z_3) + y_2(z_3 - z_1) + y_3(z_1 - z_2)$$

$$V = z_1(x_2 - x_3) + y_2(x_3 - x_1) + y_3(x_1 - x_2)$$

$$W = x_1(y_2 - y_3) + x_2(y_3 - y_1) + x_3(y_1 - y_2)$$

$$\Delta = -x_1(y_2y_3 - y_3y_2) - x_2(y_3z_1 - y_1z_3) + x_3(y_1z_2 - y_2z_1) \quad (16)$$

The target cell regions with coefficients might lie either interior or exterior to the surface [40].

The inequality range shown in (17)

$$U_x + V_y + W_z + \Delta < 0$$

$$U_x + V_y + W_z > 0 \quad (17)$$

If range is <0, then (x, y, z) with inequality lies interior to the surface, else otherwise. Parametric representation is used further to view the Cancer Detected cells in 3D. Image reconstruction is done by using a Filtering algorithm as shown in Figure 5.

Reconstructing using Filtering Algorithm
Input: Input Mesh, Boundary data, Maximum Number of Iterations Output: Number of Mean Linear Prediction values
Step 1: Read the data. Step 2: Remove NULL data. Step 3: Initialize anomaly variable. Step 4: loop iteration i) Set Phase and Amplitude part. ii) Read reference point data. iii) Calculate displacement errors. iv) Normalize parametric data with respect to optical values. v) Normalize by looping through each node, rather than creating a diagonal matrix and then multiplying. vi) Apply Filter Regularization vii) Capture the anomaly. end loop.

Fig. 5 Proposed image filtering and reconstruction algorithm

The designated points are fetched according to the calculated area of defective regions and surfaces in a 3D plane. The viewpoint coordinates are obtained after iterative inequality tests are performed. By augmenting the intensity values of images in terms of color, brightness, and sharpness, a segmented image is obtained. The different intensity values for the filtered image are obtained by using the Visual Transformer Model (VIT). The cross-attention mechanism is applied to process the transformer encoder images. The model converts the processed images into tokens where each token represents the affected area. The proposed framework using the ViT model is shown in Figure 6.

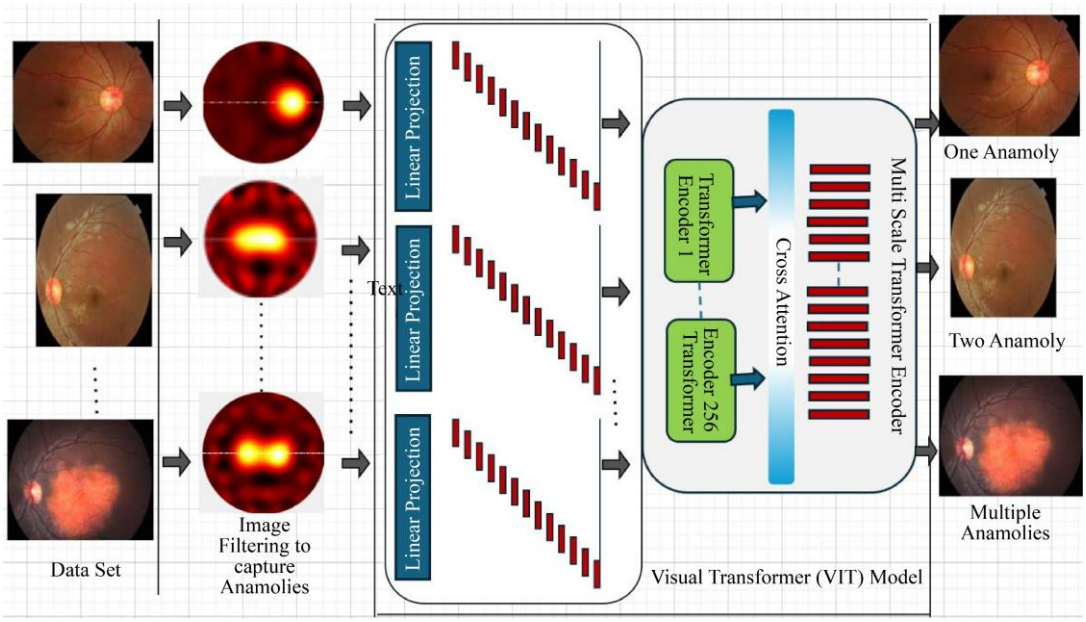

Fig. 6 Multi-scale transformer model framework

Data augmentation algorithms are applied to the training images, and rescaling is performed on the testing images. The composite data set [88-91] with 5000 images is used in the experiment with varying testing and training split (80% to 20% and 75% to 25%) and 5-fold, 10-fold cross-validation. Data generators are created using ImageDataGenerator to load and preprocess the images during model training. The implementation logic to detect and obtain anomalies is shown in Figure 7.

```
for i = 1:num
    % Define anomaly parameters
    theta = (i - 1) * (2 * pi / num); % Calculate angle for each anomaly
    anomalies(i).x = center_x + radius * cos(theta); % x position
    anomalies(i).y = center_y + radius * sin(theta); % y position
    anomalies(i).z = 0;              % z position (optional)
    anomalies(i).r = 7.5;            % radius of the anomaly
    anomalies(i).mua = 0.02;         % absorption coefficient
    anomalies(i).mus = 1;            % scatter coefficient
    anomalies(i).region = i;         % region number

    % Add anomaly to the mesh
    mesh_with_anomalies = add_blob(mesh_with_anomalies, anomalies(i));
end

%% Save Mesh with Multiple Anomalies
save_mesh(mesh_with_anomalies, 'Input_mesh_with_anomalies')

%% Plot Mesh with Multiple Anomalies
plotmesh(mesh_with_anomalies)

%% Generate Forward Data using Frequency Domain Model at 0 MHz

data_with_anomalies = femdata(mesh_with_anomalies, 0);

%% Add Random Noise (1% amplitude, and 0 degrees in Phase)

% For 1% Noise
data_with_anomalies_1per_noise = add_noise(data_with_anomalies, 1, 0);

%% Save Data
save data(data with anomalies 1per noise, 'Mesh with anomalies 1per noise data');
```

Fig. 7 Implementation logic for multiple anomalies detection

3. Results and Discussion

One anomaly detection and varying through intensity value results in the detection of the Target as shown in Figure 8.

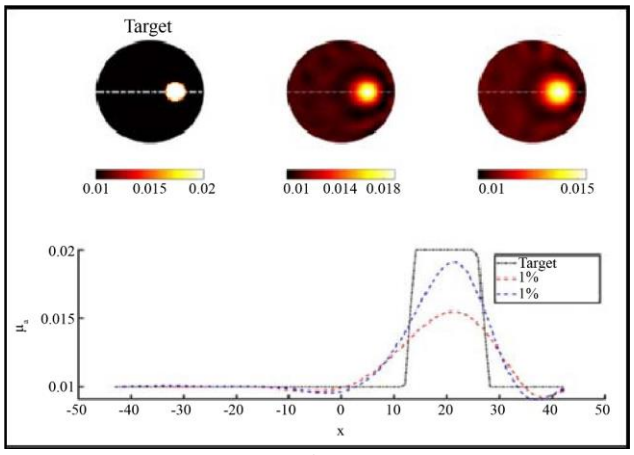

Fig. 8 One anomaly target – transformer scale applied at 5% and 1% intensity level

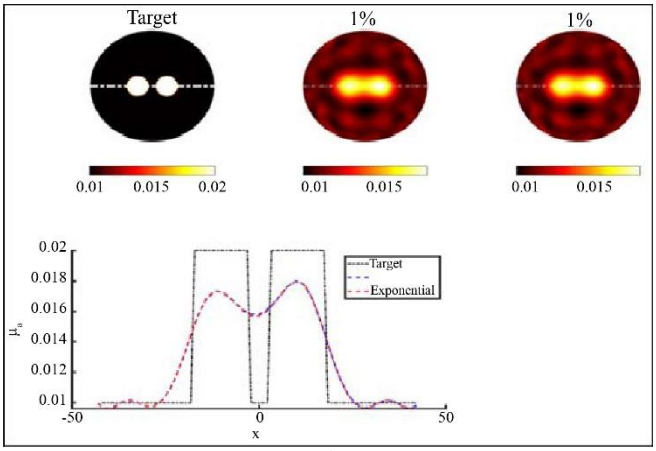

Fig. 9 Two anomaly target - transformer scale applied at multi-pass 1% intensity level

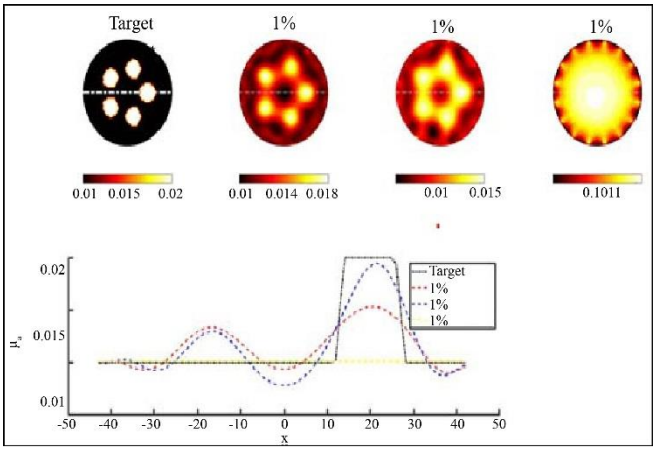

Fig. 10 Multiple anomaly target - transformer scale applied at multi pass 1% intensity level

The observation is that increasing the output dimension provides the model with greater capacity to discern intricate patterns within the data, leading to enhanced performance. The intensity values and the effect of intensity levels when the multi-scale transformation is depicted as shown in Figures 9 and 10. The detection of two and multiple anomalies is represented as shown in Figures 9 and 10, respectively. The intensity filter is applied to the generated images using multiple intensity level at 1%, 3% and 5%. To improve the quality of random and a greater number of images to detect multiple anomalies at a time, the Visual Transformation Model (ViT) framework is used.

The prediction of the categorical output data is performed on the trained data set. A data frame is created by combining the selected non-normal disease images with anomalies. The ViT model is a deeper version of the Multi-Scale Transformer architecture, and the details of the layers used for training and testing the images are shown in Figure 13. The total parameters considered are 17,943, 108. True Positive Rate can be described as a ratio between the number of correct classifications and the total number of members [41]. The ratio between correct, Ti, and incorrect classification, Tj, is written as shown in (18).

$$TFR = \frac{T_i}{T_i + T_j} \tag{18}$$

The False positive ratio between incorrect classification in he first class, $F_{j,}$ and the total number of members of the second class (F_i + F_j), $F_{i,}$ and incorrect classification, $F_{j,}$ is written as shown in (19).

$$FTR = \frac{F_i}{F_i + F_j} \tag{19}$$

The number of True Positives, False Positives, False Negatives, and True Negatives in the range of classification is easily obtained via Equations 20-23 [42].

True Positives,

$$TPi = TFRi \tag{20}$$

False Negatives,

$$FNi = \sum_{j=1}^{n} TRF_{ij} - TP_i \tag{21}$$

False Positives,

$$FP_i = \sum_{j=1}^{n} FTR_{ji} - FN_i \tag{22}$$

True Negatives,

$$TN_i = \sum_{j=1}^{n} \sum_{k=1}^{n} TRF_{ik} - TP_i - FP_i - FN_i \tag{23}$$

True Negative and True Positive are correctly classified as normal. False Positives and False Negatives are classified as incorrectly classified [42].

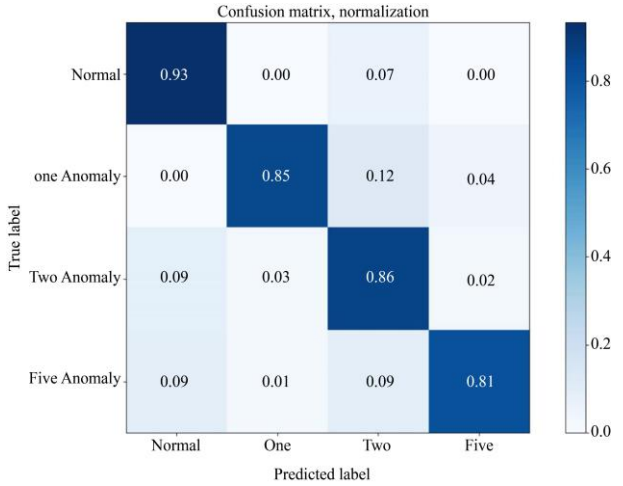

Fig. 11 Confusion matrix

Data was pre-processed by considering the class name in anomaly detection. At a time, only one type of class is classified, and other anomalies are considered as one class. A data frame consisting of both classes was created, and the image size was set to (224,224,3). Evaluation and comparison of true values with predicted values is represented through a confusion matrix. The calculation matrix is shown in Figure 11. The four parameters considered for the performance evaluation are Precision, Recall, F1-Score, and Accuracy [43]. Recall is used to provide information about how effectively the system reduces False Negatives. The F1-Score gives the model accuracy with a score representing the harmonic means of precision and recall. Accuracy is used to measure the results of true value [37]. The performance evaluation metrics are derived as per (24) to (27).

$$Precision_i = \frac{TP_i}{TP_i + FP_i} \tag{24}$$

$$Recall_i = \frac{TP_i}{TP_i + FN_i} \tag{25}$$

$$F1Score_i = \frac{2 \times TP_i}{2 \times TP_i + FP_i + FN_i} \tag{26}$$

$$Accuracy_i = \frac{TP_i}{TP_i + FP_i + FN_i + TN_i} \tag{27}$$

With the proposed ViT model, the gradient problem is significantly resolved due to the deep shallow architecture. The research is based on a multi-scale transformer algorithm of image optimization that will be used to estimate the severity of ocular disease symptoms. All methods have been compared and evaluated from a standpoint of classification performances. The weights of the pre-trained model are fine-tuned for the new data set [44]. With 768 encoding and pooling dimensions are followed by a fully connected hidden layer with 12× 12 pool size and 12 ×12 cross attention. The ReLU activation function is used by the hidden layers and in between each fully connected layer with Dense 224 layers, 16 patches, and 3 input channels. Bilinear resampling, rescale factor of 1/255, and ImageNet standard mean are applied on the processed data for further normalization of the batch of images. The classification metric is shown in Table 2.

Table 2. Classification metric

Classification Types	Precision	Recall	F1-Score	Support
Normal	0.99	0.98	0.99	416
One Anomaly	0.98	0.97	0.91	57
Two Anomaly	0.96	0.91	0.98	414
Multiple Anomalies	0.95	0.91	0.91	68

As shown in Table 2, an accuracy close to 99% is achieved after fine-tuning the proposed model. The overall Accuracy observed before fine-tuning was 86.25%. As shown in Table 3, an accuracy of 99% is achieved after stopping the missing anomalies. There was an improvement in sensitivity without increasing false alarms by fixing the class imbalance. A stronger augmentation was used to improve ViT performance to overcome confusion in anomaly types. While improving the model, it is ensured that the focal loss remains greater than cross-entropy.

Using Ensemble and removing label noise further, there was a gain observed in parameters such as Augmentation from +2 to 4%, Focal loss from +3 to 6%, Resolution from +2 to 4% and Ensemble from +3 to 6%. As a result, the ViT model is fine-tuned to achieve better overall Accuracy of upto 0.99, F1 score value of 0.99, Precision of upto 99% and Recall of upto 0.98. It can be concluded that ViT gives the highest Accuracy in predicting the kind of disease present in the human eye, provided the set is clean and balanced. So accordingly, ViT was preferred over the VGG19 [95], ResNet50 [35], FIT-Net [66], AlexNet [35], and OctNet [84] algorithms. The data frame consists of two attributes. One is an eye image, and the other is an anomaly type. An individual anomaly detection comparison for all types of anomalies is shown in the Table. 4

Table 3. Overall accuracy comparison of the proposed model with VGG19 and ResNet 50 algorithm

Model Name	Accuracy Score
ResNet 50 [35]	93.8%
FIT-Net [66]	95%
AlexNet [35]	93%
OctNet [84]	97.8%
VGG 19 Transfer Learning [95]	93%
Proposed ViT Transformer Model	99%

Table 4. Anomaly detection accuracy comparison

Anomaly Type	ResNet – 50	VGG-19	Proposed ViT Model
One Anomaly	66.67%	90%	~99%
Two Anomalies	64.58%	92.07%	96%
Multiple Anomalies	51.56%	93.75%	95%

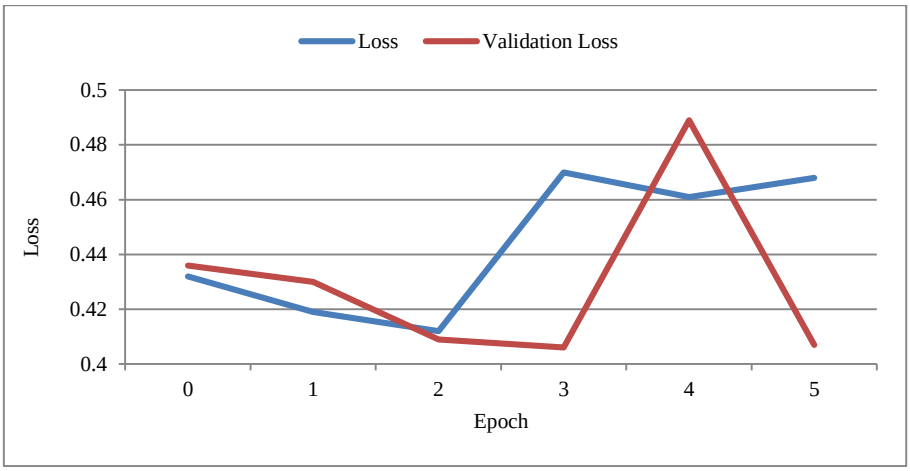

Fig. 12 ViT model loss-one anomaly

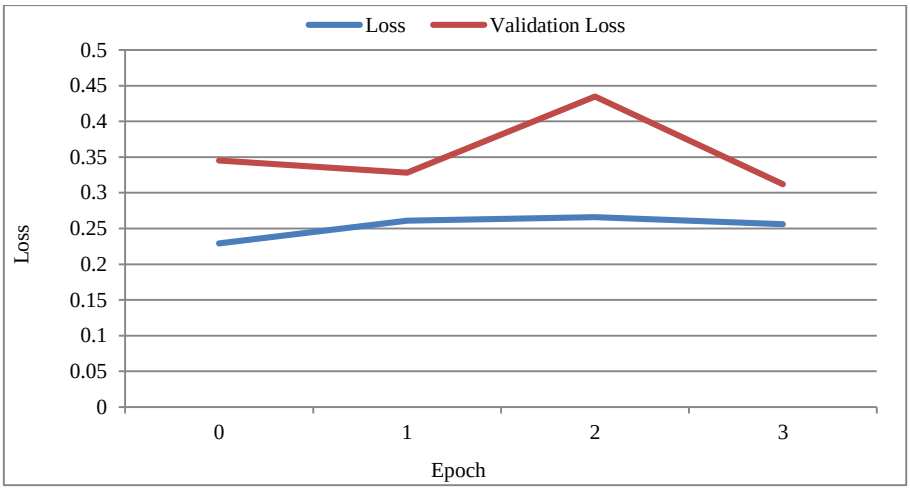

Fig. 13 ViT model loss – two anomalies

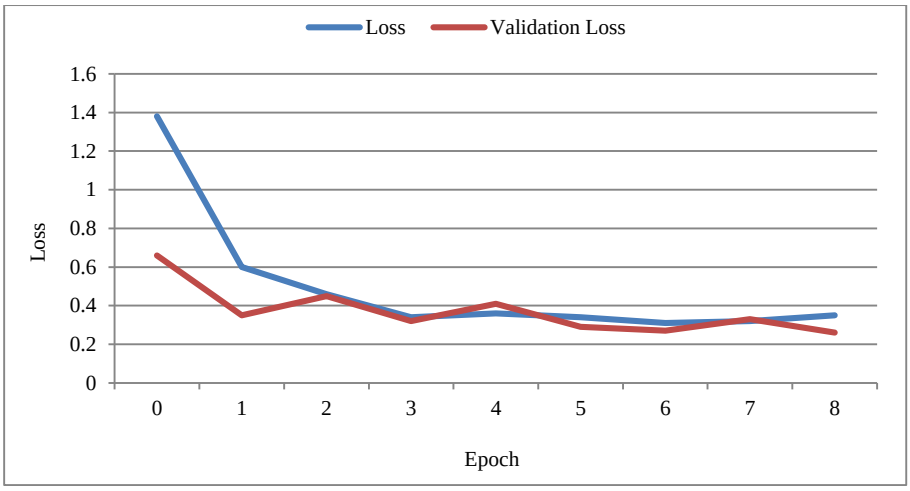

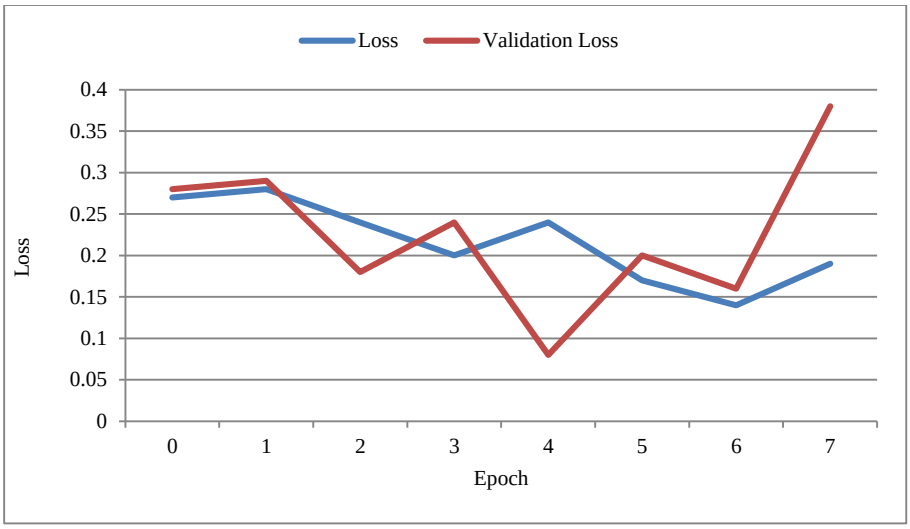

Fig. 14 ViT model loss - multiple anomalies

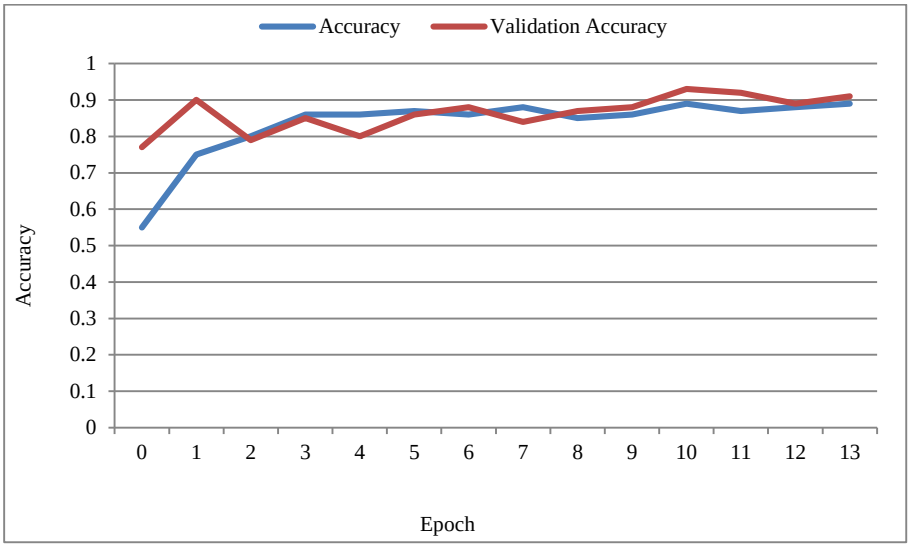

Fig. 15 ViT model accuracy - one anomaly

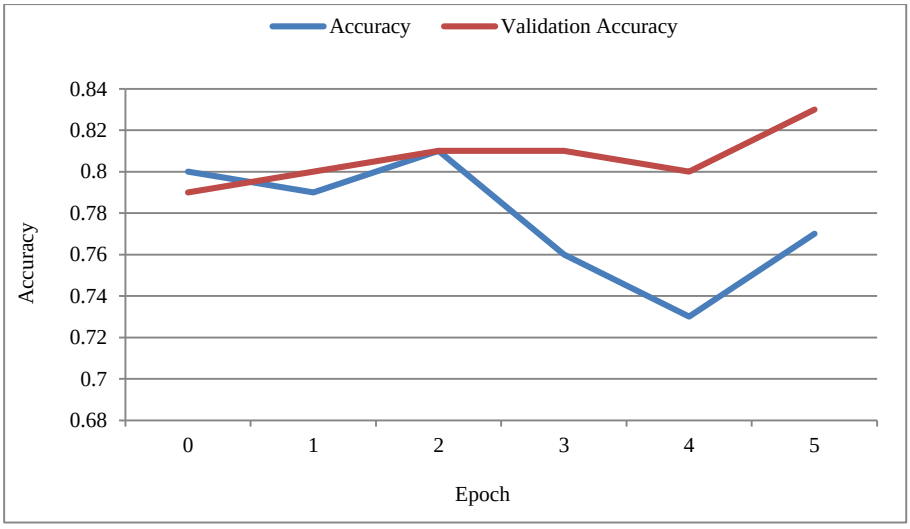

Fig. 16 ViT model accuracy - two anomalies, epoch(x-axis) and accuracy(y-axis)

Figures 12 and 13 illustrate the model loss observed for the One Anomaly and Two Anomalies categories, respectively. Figure 14 depicts the model loss observed for multiple anomaly categories. The prediction accuracy achieved is 95% for multiple anomalies. The comparison graphs are shown in Figures 15 and 16 for ViT model accuracy for individual anomaly detection types, for One Anomaly and Two Anomalies, respectively. The model accuracy graph for multiple Anomalies is shown in Figure 17. As per the result obtained, the clinical implication of the proposed approach would help in diagnosing unidentified cancer segments, as the filtering algorithm works effectively than existing approaches, as justified from Figures 18 and 19.

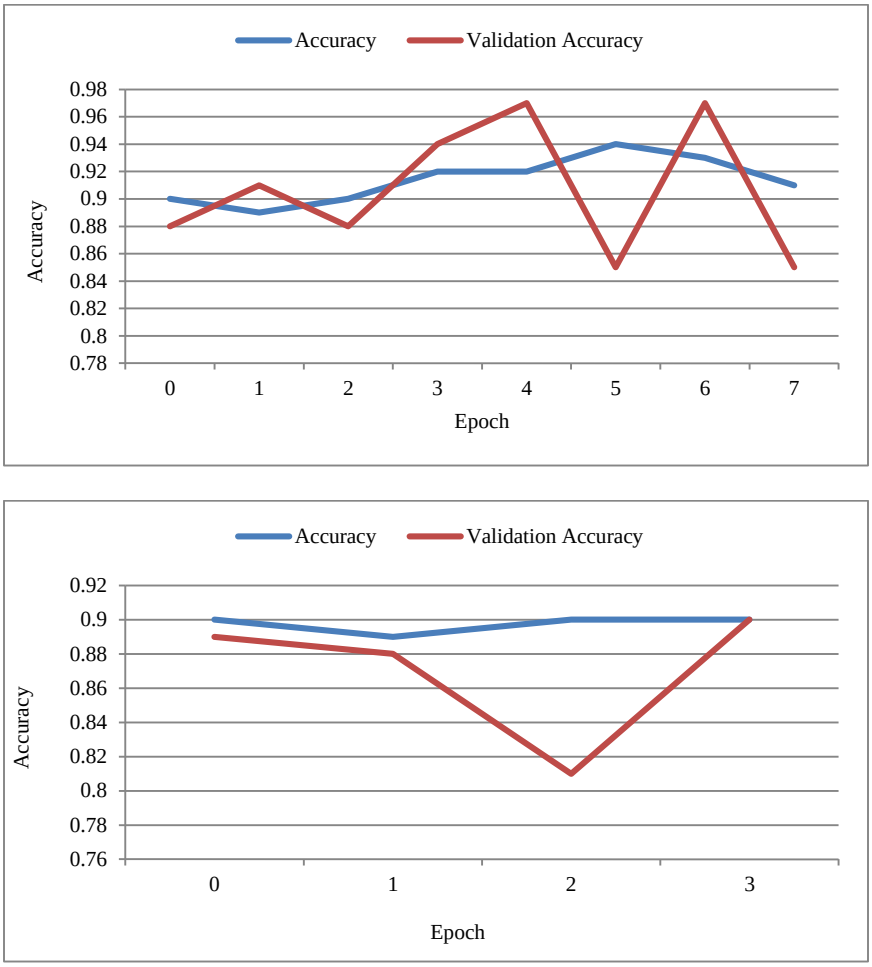

Fig. 17 ViT model accuracy for multiple anomalies, epoch(x-axis) and loss(y-axis)

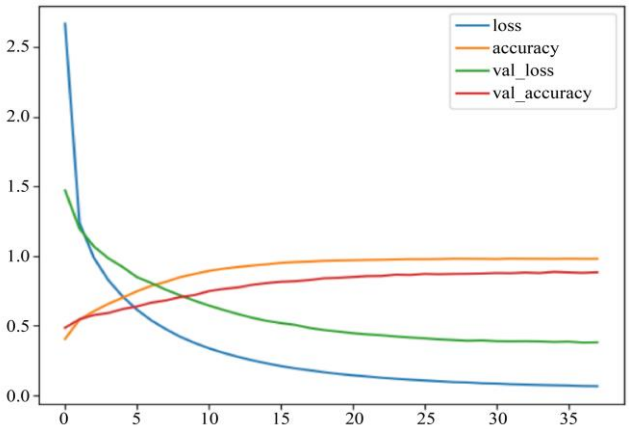

Fig. 18 ViT model overall accuracy for multiple anomalies, epoch(x-axis) and loss(y-axis), accuracy (y-axis)

Overall, model accuracy and loss are shown in Figure 18 with more than 35 epochs. With training and testing of the data set, higher accuracy and validation accuracy with less over-fitting of data are observed. Restructuring and scaling of the image is accomplished using the proposed ViT model. The comparison of Accuracy and loss between ResNet-50, proven as best in the existing approaches, and our proposed Multi-Scale Transformer-based ViT Model, along with the transfer learning model VGG19, is depicted in Figure 19. The result shows that the ViT model proves best among the existing approaches for cancer cell detection with an accuracy of 99.9%.

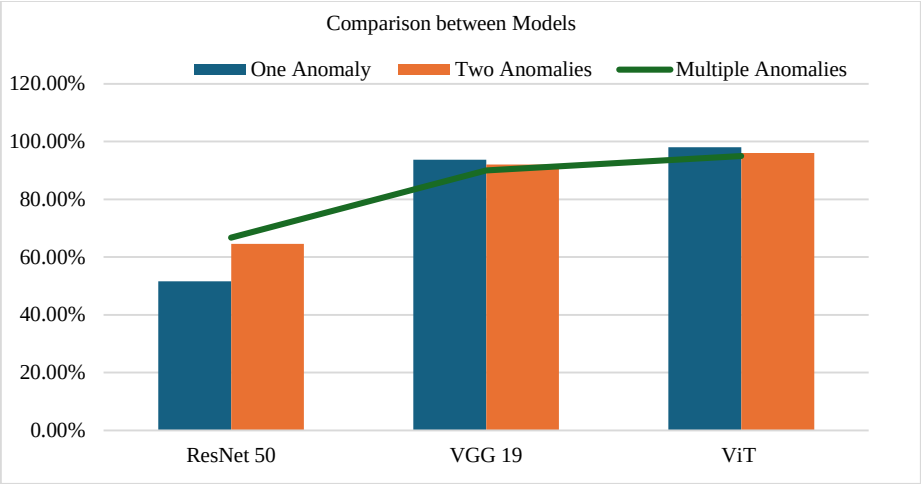

Fig. 19 Accuracy comparison between ResNet-50, VGG19 model and ViT model

4. Conclusion

Cancer cell detection is critical for the treatment of Cancer in the early stages. The traditional method of detecting ocular cancer cells consumes time, and detection is not 100 percent accurate. Fundus photography, optical coherence tomography, and clinical observation are the existing methods to detect anomalies. Image segmentation, filtering, and optimization are important to detect the infected regions of ocular cells. The Accuracy of anomaly detection can be improved by optimizing the existing methods. The result shows that with an optimized approach on processed images, the anomaly detection approach is improved by 4%. A multi-scale transformer-based framework is proposed in the paper to achieve better Accuracy in the detection of Anomalies with an overall accuracy of 99%.

References

[1] Yihong Li et al., "Improving CT Quality for Complex Objects with the Novel Autoexposure Imaging of Stepped Voltage Scanning," *IEEE Transactions on Instrumentation and Measurement*, vol. 72, pp. 1-10, 2023. [CrossRef] [Google Scholar] [Publisher Link]

[2] Behrad Fatemeh, and Abadeh Saniee Mohammad, "An Overview of Deep Learning Methods for Multimodal Medical Data Mining," *Expert Systems with Applications*, vol. 200, 2022. [CrossRef] [Google Scholar] [Publisher Link]

[3] Jing Wang et al., "Multi-Label Classification of Fundus Images with EfficientNet," *IEEE Access*, vol. 8, pp. 212499-212508, 2020. [CrossRef] [Google Scholar] [Publisher Link]

[4] M. Rizvana, and Sathiya Narayanan, "Deep Learning of Fundus Images and Optical Coherence Tomography Images for Ocular Disease Detection-A Review," *Multimedia Tools and Applications*, vol. 83, no. 41, pp. 88745-88789, 2024. [CrossRef] [Google Scholar] [Publisher Link]

[5] Mateo Gende et al., "Automatic Segmentation and Intuitive Visualisation of the Epiretinal Membrane in 3D OCT Images using Deep Convolutional Approaches," *IEEE Access*, vol. 9, pp. 75993-76004, 2021. [CrossRef] [Google Scholar] [Publisher Link]

[6] Kaveri A. Thakoor et al., "Robust and Interpretable Convolutional Neural Networks to Detect Glaucoma in Optical Coherence Tomography Images," *IEEE Transactions on Biomedical Engineering*, vol. 68, no. 8, pp. 2456-2466, 2021. [CrossRef] [Google Scholar] [Publisher Link]

[7] Min Zhou et al., "Recent Progress in Retinoblastoma: Pathogenesis, Presentation, Diagnosis and Management," *Asia-Pacific Journal of Ophthalmology*, vol. 13, no. 2, pp. 1-13, 2024. [CrossRef] [Google Scholar] [Publisher Link]

[8] Yasuyoshi Sato et al., "Squamous Cell Carcinoma of the Eyelid," *Japanese Journal of Clinical Oncology*, vol. 54, no. 1, pp. 4-12, 2023. [CrossRef] [Google Scholar] [Publisher Link]

[9] Robin Howard et al., *Toxic, Metabolic and Physical Insults to the Nervous System*, Neurology: A Queen Square Textbook, Wiley Press, pp. 903-943, 2024. [CrossRef] [Google Scholar] [Publisher Link]

[10] Peiqi Ding, Ruiqing Wang, and Yuxi He, "Risk Factors for Pterygium: Latest Research Progress on Major Pathogenesis," *Experimental Eye Research*, vol. 243, 2024. [CrossRef] [Google Scholar] [Publisher Link]
[11] Ndidi Enwereji, Madina Falcone, and Katalin Ferenczi, "Lymphoma Involvement of the Eyelid and Eye," *Clinics in Dermatology*, vol. 42, no. 4, pp. 373-380, 2024. [CrossRef] [Google Scholar] [Publisher Link]
[12] Syed Hameed et al., "Genetic Risk Factors and Clinical Outcomes in Childhood Eye Cancers: A Review," *Genes*, vol. 15, no. 3, pp. 1-21, 2024. [CrossRef] [Google Scholar] [Publisher Link]
[13] Xiaoyou Tang et al., "Current Insights and Future Perspectives of Ultraviolet Radiation (UV) Exposure: Friends and Foes to the Skin and Beyond the Skin," *Environment International*, vol. 185, pp. 1-15, 2024. [CrossRef] [Google Scholar] [Publisher Link]
[14] Shaan Lalvani, and Rebecca M Brown, "Neurofibromatosis Type 1: Optimizing Management with a Multidisciplinary Approach," *Journal of Multidisciplinary Healthcare*, vol. 17, pp. 1803-1817, 2024. [CrossRef] [Google Scholar] [Publisher Link]
[15] Wajeeha Saeed et al., "Cutaneous Oncology: Strategies for Melanoma Prevention, Diagnosis, and Therapy," *Cancer Control*, vol. 31, pp. 1-24, 2024. [CrossRef] [Google Scholar] [Publisher Link]
[16] Jennifer Liao, Robin Redmon Wright, and Gargi K. Vora, "The Decline of Basic Ophthalmology in General Medical Education: A Scoping Review and Recommended Potential Solutions," *Journal of Medical Education and Curricular Development*, vol. 11, pp. 1-22, 2024. [CrossRef] [Google Scholar] [Publisher Link]
[17] Greg M. Hammond et al., "Prognostic Factors for a Change in Eye Health or Vision: A Rapid Review," *medRxiv*, pp. 1-91, 2024. [CrossRef] [Google Scholar] [Publisher Link]
[18] J. William Harbour, "Eye Cancer: Unique Insights into Oncogenesis the Cogan Lecture," *Investigative Ophthalmology and Visual Science*, vol. 47, no. 5, pp. 1737-1745, 2006. [CrossRef] [Google Scholar] [Publisher Link]
[19] Ali Hazazi et al., "From Diagnosis to Therapy: The Transformative Role of lncRNAs in Eye Cancer Management," *Pathology-Research and Practice*, vol. 254, 2024. [CrossRef] [Google Scholar] [Publisher Link]
[20] Krzysztof Bilmin et al., "New Perspectives for Eye-Sparing Treatment Strategies in Primary Uveal Melanoma," *Cancers*, vol. 14, no. 1, pp. 1-21, 2021. [CrossRef] [Google Scholar] [Publisher Link]
[21] Mail Barbi, Richard D. Carvajal, and Craig E. Devoe, "Updates in the Management of Uveal Melanoma," *The Cancer Journal*, vol. 30, no. 2, pp. 92-101, 2024. [CrossRef] [Google Scholar] [Publisher Link]
[22] Bertil Damato, "Ocular Treatment of Choroidal Melanoma in Relation to the Prevention of Metastatic Death-A Personal View," *Progress in Retinal and Eye Research*, vol. 66, pp. 187-199, 2018. [CrossRef] [Google Scholar] [Publisher Link]
[23] Marina Vasalaki et al., "Ocular Oncology: Advances in Retinoblastoma, Uveal Melanoma and Conjunctival Melanoma," *British Medical Bulletin*, vol. 121, no. 1, pp. 107-119, 2017. [CrossRef] [Google Scholar] [Publisher Link]
[24] Roland Höllhumer, Susan Williams, and Pamela Michelow, "Ocular Surface Squamous Neoplasia: Management and Outcomes, *Eye*, vol. 35, no. 6, pp. 1562-1573, 2021. [CrossRef] [Google Scholar] [Publisher Link]
[25] Sitong Ju et al., "Personalized Treatment Concepts in Extraocular Cancer," *Advances in Ophthalmology Practice and Research*, vol. 4, no. 2, pp. 69-77, 2024. [CrossRef] [Google Scholar] [Publisher Link]
[26] Rodrigo Anguita et al., "Managing Vitreoretinal Complications in Uveal Melanoma: Surgical Treatment and Practical Considerations," *Seminars in Ophthalmology*, vol. 40, no. 8, pp. 709-718, 2025. [CrossRef] [Google Scholar] [Publisher Link]
[27] Mrittika Sen, Hakan Demirci, and Santosh G. Honavar, "Targeted Therapy in Ophthalmic Oncology: The Current Status," *Asia-Pacific Journal of Ophthalmology*, vol. 13, no. 2, pp. 1-29, 2024. [CrossRef] [Google Scholar] [Publisher Link]
[28] Sara Verbeek, and Lauren A. Dalvin, "Advances in Multimodal Imaging for Diagnosis of Pigmented Ocular Fundus Lesions," *Canadian Journal of Ophthalmology*, vol. 59, no. 4, pp. 218-233, 2024. [CrossRef] [Google Scholar] [Publisher Link]
[29] Claus Garbe et al., "European Consensus-based Interdisciplinary Guideline for Melanoma. Part 2: Treatment-Update," *European Journal of Cancer*, vol. 170, pp. 256-284, 2022. [CrossRef] [Google Scholar] [Publisher Link]
[30] Merve Kulbay et al., "Uveal Melanoma: Comprehensive Review of Its Pathophysiology, Diagnosis, Treatment, and Future Perspectives," *Biomedicines*, vol. 12, no. 8, pp. 1-29, 2024. [CrossRef] [Google Scholar] [Publisher Link]
[31] Lamprini Banou et al., "Radiotherapy in Uveal Melanoma: A Review of Ocular Complications," *Current Oncology*, vol. 30, no. 7, pp. 6374-6396, 2023. [CrossRef] [Google Scholar] [Publisher Link]
[32] Yating Liu et al., "Personalized Treatment Approaches in Intraocular Cancer," *Advances in Ophthalmology Practice and Research*, vol. 4, no. 3, pp. 112-119, 2024. [CrossRef] [Google Scholar] [Publisher Link]
[33] Olivia J. Rolfe et al., "Combined Photodynamic Therapy and Transpupillary Thermotherapy for Small Choroidal Melanoma," *Canadian Journal of Ophthalmology*, vol. 59, no. 6, pp. 409-416, 2024. [CrossRef] [Google Scholar] [Publisher Link]
[34] Federica Dini et al., "Periocular Sebaceous Carcinoma: Updates in the Diagnosis, Treatment, Staging, and Management," *International Journal of Dermatology*, vol. 63, no. 6, pp. 726-736, 2024. [CrossRef] [Google Scholar] [Publisher Link]
[35] Isaac Arias-Serrano et al., "Artificial Intelligence based Glaucoma and Diabetic Retinopathy Detection using MATLAB-Retrained AlexNet Convolutional Neural Network," *F1000Research*, vol. 12, pp. 1-30, 2024. [CrossRef] [Google Scholar] [Publisher Link]

[36] Adwaita Nag, and Vikas Khetan, "Retinoblastoma-A Comprehensive Review, Update and Recent Advances," *Indian Journal of Ophthalmology*, vol. 72, no. 6, pp. 778-788, 2024. [CrossRef] [Google Scholar] [Publisher Link]
[37] Kristina Joana Schoelles, and Claudia Auw-Haedrich, "Updates on Eyelid Cancers," *Asia-Pacific Journal of Ophthalmology*, vol. 13, no. 2, pp. 1-15, 2024. [CrossRef] [Google Scholar] [Publisher Link]
[38] Qirat Qurban, and Lorraine Cassidy, "Artificial Intelligence and Machine Learning a New Frontier in the Diagnosis of Ocular Adnexal Tumors: A Review," *SAGE Open Medicine*, vol. 12, pp. 1-8, 2024. [CrossRef] [Google Scholar] [Publisher Link]
[39] Adrienne B. Shannon, Jonathan S. Zager, and Matthew C. Perez, "Clinical Characteristics and Special Considerations in the Management of Rare Melanoma Subtypes," *Cancers*, vol. 16, no. 13, pp. 1-20, 2024. [CrossRef] [Google Scholar] [Publisher Link]
[40] Andrea Boutros et al., "The Treatment of Advanced Melanoma: Current Approaches and New Challenges," *Critical Reviews in Oncology/Hematology*, vol. 196, pp. 1-15, 2024. [CrossRef] [Google Scholar] [Publisher Link]
[41] Zhengwei Zhang, Callie Deng, and Yannis M. Paulus, "Advances in Structural and Functional Retinal Imaging and Biomarkers for Early Detection of Diabetic Retinopathy," *Biomedicines*, vol. 12, no. 7, pp. 1-28, 2024. [CrossRef] [Google Scholar] [Publisher Link]
[42] Junwoo Kim et al., "Advances in Cellular and Tissue-based Imaging Techniques for Sarcoid Granulomas," *American Journal of Physiology-Cell Physiology*, vol. 326, no. 1, pp. C10-C26, 2023. [CrossRef] [Google Scholar] [Publisher Link]
[43] John Apps et al., "A Review Calling for Research Directed at Early Detection of Childhood Cancers: The Clinical, Scientific, and Economic Arguments for Population Screening and Surveillance," *EJC Paediatric Oncology*, vol. 4, pp. 1-8, 2024. [CrossRef] [Google Scholar] [Publisher Link]
[44] Michael Balas et al., "Adaptive Optics Imaging in Ophthalmology: Redefining Vision Research and Clinical Practice," *JFO Open Ophthalmology*, vol. 7, pp. 1-11, 2024. [CrossRef] [Google Scholar] [Publisher Link]
[45] Minnu Varghese, Sony Varghese, and S. Preethi, "Revolutionizing Medical Imaging: A Comprehensive Review of Optical Coherence Tomography (OCT)," *Journal of Optics*, vol. 54, no. 3, pp. 1178-1195, 2024. [CrossRef] [Google Scholar] [Publisher Link]
[46] Mohammed Yusuf Ansari et al., "Advancements in Deep Learning for B-Mode Ultrasound Segmentation: A Comprehensive Review," *IEEE Transactions on Emerging Topics in Computational Intelligence*, vol. 8, no. 3, pp. 2126-2149, 2024. [CrossRef] [Google Scholar] [Publisher Link]
[47] Anne Helene K. Nissen, and Anna Stage Vergmann, "Clinical Utilisation of Wide-Field Optical Coherence Tomography and Angiography: A Narrative Review," *Ophthalmology and Therapy*, vol. 13, no. 4, pp. 903-915, 2024. [CrossRef] [Google Scholar] [Publisher Link]
[48] Zoe Gabrielle Attal et al., "Advanced and Metastatic Non-Melanoma Skin Cancer: Epidemiology, Risk Factors, Clinical Features, and Treatment Options," *Biomedicines*, vol. 12, no. 7, pp. 1-17, 2024. [CrossRef] [Google Scholar] [Publisher Link]
[49] Lai WEI, and Menghan HU, "A Review of Medical Ocular Image Segmentation," *Virtual Reality and Intelligent Hardware*, vol. 6, no. 3, pp. 181-202, 2024. [CrossRef] [Google Scholar] [Publisher Link]
[50] Nishita Kalra, Prachi Verma, and Surajpal Verma, "Advancements in AI based Healthcare Techniques with FOCUS ON Diagnostic Techniques," *Computers in Biology and Medicine*, vol. 179, 2024. [CrossRef] [Google Scholar] [Publisher Link]
[51] Saad Islam et al., "Retinal Health Screening using Artificial Intelligence with Digital Fundus Images: A Review of the Last Decade (2012-2023)," *IEEE Access*, vol. 12, pp. 176630-176685, 2024. [CrossRef] [Google Scholar] [Publisher Link]
[52] Aniket Patil, Anjula Mehto, and Saif Nalband, "Enhancing Skin Lesion Diagnosis with Data Augmentation Techniques: A Review of the State-of-the-Art," *Multimedia Tools and Applications*, vol. 84, no. 22, pp. 25325-25364, 2025. [CrossRef] [Google Scholar] [Publisher Link]
[53] Fangping Wan et al., "Machine Learning for Antimicrobial Peptide Identification and Design," *Nature Reviews Bioengineering*, vol. 2, no. 5, pp. 392-407, 2024. [CrossRef] [Google Scholar] [Publisher Link]
[54] Simon Schürer-Waldheim et al., "Robust Fovea Detection in Retinal OCT Imaging using Deep Learning," *IEEE Journal of Biomedical and Health Informatics*, vol. 26, no. 8, pp. 3927-3937, 2022. [CrossRef] [Google Scholar] [Publisher Link]
[55] Mohan Anand, and Sundaram Meenakshi, "Channel and Spatial Attention Aware UNet Architecture for Segmentation of Blood Vessels, Exudates and Microaneurysms in Diabetic Retinopathy," *Research Square*, 2023. [CrossRef] [Google Scholar] [Publisher Link]
[56] Gen Miura et al., "Ocular Syphilis with Optic Disc Neovascularization Treated with Bevacizumab Evaluated by OCT Angiography and Electroretinography," *Journal of Ophthalmic Inflammation and Infection*, vol. 10, no. 1, pp. 1-5, 2020. [CrossRef] [Google Scholar] [Publisher Link]
[57] Harshit Kaushik et al., "Diabetic Retinopathy Diagnosis from Fundus Images using Stacked Generalization of Deep Models," *IEEE Access*, vol. 9, pp. 108276-108292, 2021. [CrossRef] [Google Scholar] [Publisher Link]
[58] Gaurav Singh et al., "A Comprehensive Assessment of Artificial Intelligence Applications for Cancer Diagnosis," *Artificial Intelligence Review*, vol. 57, no. 7, pp. 1-52, 2024. [CrossRef] [Google Scholar] [Publisher Link]
[59] Ye Eun Han et al., "Choroidal Manifestations of Non-Ocular Sarcoidosis: An Enhanced Depth Imaging OCT Study," *BMC Ophthalmology*, vol. 24, no. 1, pp. 1-9, 2024. [CrossRef] [Google Scholar] [Publisher Link]

[60] Tong Zhang et al., "Compressive Spectral X-Ray CT Reconstruction via Deep Learning," *IEEE Transactions on Computational Imaging*, vol. 8, pp. 1038-1050, 2022. [CrossRef] [Google Scholar] [Publisher Link]

[61] Giovanni Mettivier et al., "In-Line Phase Contrast Mammography, Phase Contrast Digital Breast Tomosynthesis, and Phase Contrast Breast Computed Tomography with a Dedicated CT Scanner and a Microfocus X-Ray Tube: Experimental Phantom Study," *IEEE Transactions on Radiation and Plasma Medical Sciences*, vol. 5, no. 6, pp. 793-806, 2021. [CrossRef] [Google Scholar] [Publisher Link]

[62] Burak Kucukgoz et al., "Deep Learning using Preoperative Optical Coherence Tomography Images to Predict Visual Acuity Following Surgery for Idiopathic Full-Thickness Macular Holes," *IEEE Access*, vol. 12, pp. 32911-32926, 2024. [CrossRef] [Google Scholar] [Publisher Link]

[63] Laith Alzubaidi et al., "Review of Deep Learning: Concepts, CNN Architectures, Challenges, Applications, Future Directions," *Journal of Big Data*, vol. 8, no. 1, pp. 1-74, 2021. [CrossRef] [Google Scholar] [Publisher Link]

[64] Sumaiya Thaseen Ikram et al., "Anomaly Detection using XGBoost Ensemble of Deep Neural Network Models," *Cybernetics and Information Technologies*, vol. 21, no. 3, pp. 175-188, 2021. [CrossRef] [Google Scholar] [Publisher Link]

[65] Parisa Ghaderi Daneshmand, and Hossein Rabbani, "Tensor Ring Decomposition Guided Dictionary Learning for OCT Image Denoising," *IEEE Transactions on Medical Imaging*, vol. 43, no. 7, pp. 2547-2562, 2024. [CrossRef] [Google Scholar] [Publisher Link]

[66] Shaobin Chen et al., "FIT-Net: Feature Interaction Transformer Network for Pathologic Myopia Diagnosis," *IEEE Transactions on Medical Imaging*, vol. 42, no. 9, pp. 2524-2538, 2023. [CrossRef] [Google Scholar] [Publisher Link]

[67] Mythili Thirugnanam, and S. Margret Anouncia, "Evaluating the Performance of Various Segmentation Techniques in Industrial Radiographs," *Cybernetics and Information Technologies*, vol. 14, no. 1, pp. 161-171, 2014. [CrossRef] [Google Scholar] [Publisher Link]

[68] Omar Bernabé et al., "Classification of Eye Diseases in Fundus Images," *IEEE Access*, vol. 9, pp. 101267-101276, 2021. [CrossRef] [Google Scholar] [Publisher Link]

[69] Sai Li et al., "Application of Semi-Supervised Learning in Image Classification: Research on Fusion of Labeled and Unlabeled Data," *IEEE Access*, vol. 12, pp. 27331-27343, 2024. [CrossRef] [Google Scholar] [Publisher Link]

[70] Mohamed Elsharkawy et al., "A Clinically Explainable AI-based Grading System for Age-Related Macular Degeneration using Optical Coherence Tomography," *IEEE Journal of Biomedical and Health Informatics*, vol. 28, no. 4, pp. 2079-2090, 2024. [CrossRef] [Google Scholar] [Publisher Link]

[71] Andreas S. Panayides et al., "AI in Medical Imaging Informatics: Current Challenges and Future Directions," *IEEE Journal of Biomedical and Health Informatics*, vol. 24, no. 7, pp. 1837-1857, 2020. [CrossRef] [Google Scholar] [Publisher Link]

[72] Guangming Ni et al., "Toward Ground-Truth Optical Coherence Tomography via Three-Dimensional Unsupervised Deep Learning Processing and Data," *IEEE Transactions on Medical Imaging*, vol. 43, no. 6, pp. 2395-2407, 2024. [CrossRef] [Google Scholar] [Publisher Link]

[73] Buxin Chen et al., "Accurate Reconstruction of Multiple Basis Images Directly from Dual-Energy Data in CT," *IEEE Transactions on Biomedical Engineering*, vol. 71, no. 7, pp. 2058-2069, 2024. [CrossRef] [Google Scholar] [Publisher Link]

[74] Yating Ling et al., "MTANet: Multi-Task Attention Network for Automatic Medical Image Segmentation and Classification," *IEEE Transactions on Medical Imaging*, vol. 43, no. 2, pp. 674-685, 2024. [CrossRef] [Google Scholar] [Publisher Link]

[75] Amit Bhati et al., "Discriminative Kernel Convolution Network for Multi-Label Ophthalmic Disease Detection on Imbalanced Fundus Image Dataset," *Computers in Biology and Medicine*, vol. 153, pp. 1-8, 2023. [CrossRef] [Google Scholar] [Publisher Link]

[76] Kari Venkatram, and Mary A. Geetha, "Review on Big Data and Analytics-Concepts, Philosophy, Process and Applications," *Cybernetics and Information Technologies*, vol. 17, no. 2, pp. 3-27, 2017. [CrossRef] [Google Scholar] [Publisher Link]

[77] Xuan Yuwen et al., "An Improved Strategy for Active Visual Odometry based on Robust Adaptive Unscented Kalman Filter," *IEEE Transactions on Industrial Electronics*, vol. 71, no. 8, pp. 9172-9181, 2024. [CrossRef] [Google Scholar] [Publisher Link]

[78] Mohinder S. Grewal, and Angus P. Andrews, *Kalman Filtering: Theory and Practice with MATLAB*, John Wiley and Sons, 2015. [CrossRef] [Google Scholar] [Publisher Link]

[79] Fernando Matía et al., "The fuzzy Kalman filter: Improving its Implementation by Reformulating Uncertainty Representation," *Fuzzy Sets and Systems*, vol. 402, pp. 78-104, 2021. [CrossRef] [Google Scholar] [Publisher Link]

[80] Hermes H. Ferreira, and Eduardo S.L. Gastal, "Efficient 2D Tikhonov Smoothness Regularization with Recursive Filtering," *Pattern Recognition Letters*, vol. 175, pp. 95-103, 2023. [CrossRef] [Google Scholar] [Publisher Link]

[81] Jason T. Smith et al., "Deep Learning in Macroscopic Diffuse Optical Imaging," *Journal of Biomedical Optics*, vol. 27, no. 2, pp. 1-26, 2022. [CrossRef] [Google Scholar] [Publisher Link]

[82] Kaiming He et al., "Deep Residual Learning for Image Recognition," *Proceedings of the IEEE Conference on Computer Vision and Pattern Recognition*, pp. 770-778, 2016. [Google Scholar] [Publisher Link]

[83] Cecilia S. Lee et al., "Deep Learning is Effective for Classifying Normal Versus Age-Related Macular Degeneration OCT Images," *Ophthalmology Retina*, vol. 1, no. 4, pp. 322-327, 2017. [CrossRef] [Google Scholar] [Publisher Link]

[84] Jin Qian et al., "Classifying Retinal Diseases Via Pyramid Vision Graph Convolutional Network for Optical Coherence Tomography Images," *Biomedical Optics Express*, vol. 16, no. 6, pp. 2312-2326, 2025. [CrossRef] [Google Scholar] [Publisher Link]

[85] Ho Law et al., "Quasiconformal Model with CNN Features for Large Deformation Image Registration," *American Institute of Mathematical Science*, vol. 16, no. 4, pp. 1019-1046, 2020. [CrossRef] [Google Scholar] [Publisher Link]

[86] Daiki Nishigaki et al., "Vision Transformer to Differentiate Between Benign and Malignant Slices in ^{18}F-FDG PET/CT," *Scientific Reports*, vol. 14, no. 1, pp. 1-11, 2024. [CrossRef] [Google Scholar] [Publisher Link]

[87] Gaurav Khanduja, "*Multiple Dataset Visualization (MDV) Framework for Scalar Volume Data*," Louisiana State University and Agricultural and Mechanical College ProQuest Dissertations and Theses, pp. 1-148, 2009. [CrossRef] [Google Scholar] [Publisher Link]

[88] Ning Li et al., "A Benchmark of Ocular Disease Intelligent Recognition: One Shot for Multi-Disease Detection," *Benchmarking, Measuring, and Optimizing: Third BenchCouncil International Symposium, Bench 2020, Virtual Event*, Springer, Cham, pp. 177-193, 2021. [CrossRef] [Google Scholar] [Publisher Link]

[89] S. Saravanan et al., "Explainable Artificial Intelligence (EXAI) Models for Early Prediction of Parkinson's Disease based on Spiral and Wave Drawings," *IEEE Access*, vol. 11, pp. 68366-68378, 2023. [CrossRef] [Google Scholar] [Publisher Link]

[90] Tanner Gilbert, Detectron 2, Object Detection with PyTorch, 2019. [Online]. Available: https://gilberttanner.com/blog/detectron-2-object-detection-with-pytorch/

[91] Lie Ju et al., "Hierarchical Knowledge Guided Learning for Real-World Retinal Disease Recognition," *IEEE Transactions on Medical Imaging*, vol. 43, no. 1, pp. 335-350, 2024. [CrossRef] [Google Scholar] [Publisher Link]

[92] Oscar Perdomo et al., "Classification of Diabetes-Related Retinal Diseases using a Deep Learning Approach in Optical Coherence Tomography," *Computer Methods and Programs in Biomedicine*, vol. 178, pp. 181-189, 2019. [CrossRef] [Google Scholar] [Publisher Link]

[93] Gaurav Meena, Krishna Kumar Mohbey, and Sunil Kumar, "Monkeypox Recognition and Prediction from Visuals using Deep Transfer Learning-based Neural Networks," *Multimedia Tools and Applications*, vol. 83, no. 28, pp. 71695-71719, 2024. [CrossRef] [Google Scholar] [Publisher Link]

[94] Mohaimenul Azam Khan Raiaan et al., "A Lightweight Robust Deep Learning Model Gained High Accuracy in Classifying a Wide Range of Diabetic Retinopathy Images," *IEEE Access*, vol. 11, pp. 42361-42388, 2023. [CrossRef] [Google Scholar] [Publisher Link]

[95] Wilwer J. Jaimes et al., "Detection of Retinal Diseases from OCT Images using a VGG16 and Transfer Learning," *Discover Applied Sciences*, vol. 7, no. 3, pp. 1-14, 2025. [CrossRef] [Google Scholar] [Publisher Link]